Micromagnetic simulation of magnetization reversal process and stray field behavior in Fe thin film wire

Munekazu Ohno[a)]
Research Center for Integrated Quantum Electronics, Hokkaido University, Sapporo, 060-8628, Japan

Kanji Yoh
Research Center for Integrated Quantum Electronics, Hokkaido University, Sapporo, 060-8628, Japan and CREST-JST, Kawaguchi, Saitama 332-0022, Japan

(Received 17 May 2007; accepted 15 October 2007; published online 28 December 2007)

The magnetization reversal process of Fe thin film wire is studied based on two-dimensional micromagnetic simulation. It is demonstrated that the external field parallel to the width direction results in the formation of a 180° Néel wall, whereas the field applied to the thickness direction yields the Bloch-like walls, which turn into *C*-type walls in the residual state. These behaviors are explained by the anisotropic dependence of wall energy in the direction of the external field. The stray field during this process is analyzed in detail. © *2007 American Institute of Physics*.
[DOI: 10.1063/1.2821731]

I. INTRODUCTION

Ferromagnetic metal/semiconductor (FM/SC) hybrid structure has been attracting great attention in the field of spintronics as a candidate for use in spin-related devices, such as spin transistor.[1–3] The Fe/InAs structure is among the most promising FM/SC structures enabling decent Ohmic contact without thermal reaction process at the interface.[4] A recent work by Yoh *et al.*[5] has demonstrated the possibility of realizing a high efficient spin injection in the Fe/InAs structure. It is to be noted that micromagnetic details, such as magnetic domain pattern and domain wall structure in ferromagnetic electrode, are of critical relevance to the spin injection phenomena. The high efficient spin injection in Ref. 5 has been observed in a device with the electrode consisting of Fe thin film wire with a thickness of 30–40 nm and a width of 1–2 μm. Although an accurate estimation on spin injection efficiency requires quantitative knowledge about the external field dependence of the micromagnetic state in the electrode, such field dependence in the Fe thin film wire employed in Ref. 5 remains to be clarified.

The experimental observation of the external field dependence of a magnetic domain structure in a ferromagnetic thin film generally involves a technical difficulty to measure a weak magnetic contrast at a finite external field and most of the domain imaging studies for the Fe film have been carried out at zero external field.[6–11] Although domain patterns in the Fe film as a function of the field have been successfully investigated in recent works by means of Lorentz electron microscopy,[12–14] magnetic force microscopy (MFM),[15] and magneto-optic microscopy,[16] the microscopic details of domain wall structure and its stability under the external field have not been experimentally scrutinized. The micromagnetic simulation has been recognized as a powerful method to describe/predict the micromagnetic phenomena within a continuum system.[17–21] In this article, we report the micromagnetic simulation for the magnetization reversal process in the Fe thin film wire utilized in Ref. 5.

A number of micromagnetic simulations have been performed for the Fe thin films,[6,7,9,22–31] focusing on the most stable domain wall structure at zero external field. Several micromagnetic simulations have revealed that *C*-type wall, i.e., the Bloch-like in the interior of film and the Néel-like near the surface, is the most stable 180° wall structure in the Fe thin film with a wide range of film thickness 60–3800 nm (Refs. 7, 22, 24, and 28) and the Néel wall structure is stable in the film with smaller thickness.[9,31] It should be noted that the character of the wall structure is essentially dependent on the external field. The micromagnetic simulation for Permalloy with 50 nm thickness[32] has indicated that domain wall transition from asymmetric Bloch (*C*-type) wall to Néel wall occurs with increasing the external field in the in-plane hard axis. Although there have been several simulation studies on the magnetization reversal process for the Fe films,[21,33] the main concern in these studies was placed on the evolution/devolution of domain pattern and, to the best of authors' knowledge, the field dependence of wall character in Fe thin film has not been seriously addressed yet. The particular attention in this study is thus directed to the dependence of wall structure on the field strength and direction.

The quantitative information on the stray field associated with the micromagnetic state in the ferromagnet provides a fundamental information in the MFM analysis on the micromagnetic state and in designing a spin-related device structure. The calculation of stray field stemming from a given micromagnetic state of ferromagnetic electrode has been reported for Permalloy thin film,[34] MnAs stripe,[35] and Fe thin film.[21,31] The stray field behavior due to the existence of domain walls[31,34] and the hysteresis curve of spatially averaged stray field under the external field[21] have been analyzed in detail. In the present study, the spatial profile and the hysteresis behavior of the local stray field during the magnetization reversal process of the Fe thin film wire are com-

[a)]Electronic mail: munekazuohno76@hotmail.com.

puted. It will be demonstrated that the formation of domain wall and the domain wall transition are quite sensitively manifested in the stray field behavior.

The organization of the present article is as follows. The computational details are presented in Sec. II, followed by the calculated results and discussions in the Sec. III. We first identify the type of the most stable domain wall in the Fe thin film wire at zero external field. Our attention is then directed to the magnetization reversal process under the external field. It is shown that the external field applied to the width direction yields 180° Néel wall, whereas the field parallel to the thickness direction leads to the formation of 180° *C*-type and Bloch-like walls. These behavior are discussed in light of anisotropic dependence of wall energy on direction of the field. Then we discuss the stray field behavior during these magnetization reversal processes and the summary is given in the final section,

II. COMPUTATIONAL DETAILS

Within the micromagnetics, the magnetization vector distribution $\mathbf{M}(\mathbf{r})$ has a constant magnitude given as the saturation value, M_s, over the whole system and the main concern is placed on the direction of the local magnetization vector, more precisely, a unit vector defined as $\mathbf{M}(\mathbf{r})/M_s=(m_x,m_y,m_z)$.[18] The total energy of the system, which is a functional of m_x, m_y, and m_z, consists of the exchange energy, crystalline anisotropy energy, demagnetization energy, and Zeeman energy.[18] In the present calculation, we employed the following values for Fe,[36] saturation value of the magnetization vector, $J_s=\mu_0 M_s=2.15$ T, exchange stiffness constant, $A_0=2.5\times10^{-11}$ J/m, cubic anisotropy constant, $K_0=4.6\times10^3$ J/m^3. Our focus in this study is two-dimensional simulation for the Fe film wire and, accordingly, we used the LaBonte's expression for the demagnetization energy.[37]

The energy minimization was performed by numerically integrating the Landau–Lifshitz–Gilbert (LLG) equation[18] based on simple forward difference method with $\Delta t \sim 0.1$ ps, which is sufficiently small to avoid numerical instability. The stopping criterion for steady state is given as $|m_i(t+\Delta t)-m_i(t)|\leq 10^{-4}$ for three direction cosines at all spatial points. In preliminary calculations, we also performed the energy minimization based on the relaxation method employed in Ref. 37 and observed that there was no virtual difference in the stable domain wall structures at zero field obtained from the relaxation method and the LLG integration. The detailed comparison between the solutions by the LLG equation and the relaxation method can be found in Ref. 30.

As we employed our self-written code, the reliability of our calculation has to be mentioned here. It is first stressed that the focus of this code is a two-dimensional $x-y$ system with infinite length along the z direction. Hence, the reliability of this code cannot be tested by the μMag standard problems of the National Institute of Standards and Technology of which focuses are three-dimensional finite bodies.[38,39] Instead, we observed that our self-written code successfully reproduces the domain wall structure given in Fig. 3 of Ref. 37. Also, the preliminary calculations using our code demonstrated that the *C*-type wall is the most stable 180° domain wall structure in the Fe film with a wide range of thickness from 145 to 500 nm as is consistent with the reported works of Refs. 22 and 24. In addition, we performed several preliminary calculations using the different self-written codes for three-dimensional calculations based on the demagnetization energy expression in Ref. 40. It was demonstrated that several results shown in this article (such as Figs. 2–5) were almost identical to the ones obtained from such three-dimensional codes with employing the same calculation condition, but assigning a finite value to the z direction of element cell edge (typically 20 mm) and periodic boundary condition along the z direction. As the three-dimensional simulation for the Fe thin film wire of our interest requires an arbitrary value to be assigned to size of element cell along the z direction, we present the results obtained from the two-dimensional code based on LaBonte's demagnetization energy expression.

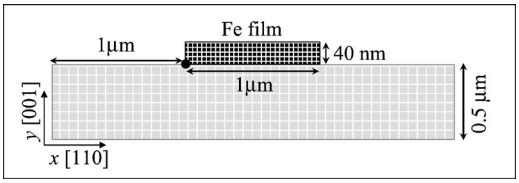

FIG. 1. Schematic picture of a two-dimensional system for the present simulation. The Fe thin film wire of 1 μm$\times$40 nm is placed at the top of a spatial coordinate (or vacuum) of 3×0.5 μm. The origin of the spatial coordinates corresponds to the edge of film as indicated by black circle.

Figure 1 schematically represents a two-dimensional system of the present concern. The Fe thin film wire with a thickness of 40 nm and a width of 1 μm is placed on the top of semiconductor (or vacuum) region. The thickness direction (y direction) corresponds to the [001] direction of bcc-Fe, whereas the width direction (x direction) is [110]. In the micromagnetic simulation, a rough discretization of computational region leads to a large error in a calculated result.[19,41] It has been recommended that the computational element size should be smaller than the stray field exchange length $(2A_0/(\mu_0 M_s^2))^{1/2}$ and also the wall width parameter $(A_0/K_0)^{1/2}$ to achieve sufficiently high accuracy.[41] These are calculated to be $(2A_0/(\mu_0 M_s^2))^{1/2}=3.42$ nm and $(A_0/K_0)^{1/2}=73.72$ nm for Fe. In all the calculations in this study, we used a two-dimensional element size of 2.5×2.5 nm and, accordingly, the computational region is divided into 400×16 element cells with a Neumann boundary condition applied to the surface cells.

The gray region (vacuum) in Fig. 1 represents the computational region for the stray field originating from the Fe thin film wire. The analytic expression for the stray field of a rectangular ferromagnet with a constant magnetization has been recently derived in Ref. 42 and this expression has been applied to the stray field calculation for a nonuniform magnetization pattern by simple superposition in Ref. 35. In this study, we calculate the stray field for the Fe thin film wire at the external field based on this expression.

TABLE I. Total energy of domain walls per unit area $E_{tot}(10^{-3}\ J/m^2)$ and the contribution of the exchange E_{ex}, crystalline anisotropy E_{an}, and demagnetization energies E_{demag}.

Domain wall	E_{tot}	E_{ex}	E_{an}	E_{demag}
Bloch	2.0110	0.6022	0.7022	0.7066
Néel	1.5447	0.2304	0.5271	0.7872
C-type	1.8686	0.6061	0.7049	0.5577

III. RESULTS AND DISCUSSIONS

A. Most stable domain wall at zero external field

Without the external field, the ground state of magnetization vector distribution in the Fe thin film wire corresponds to the state with all the magnetization vectors uniformly pointing to the z direction (the $[1\bar{1}0]$ direction of bcc-Fe in the present structure), which has been confirmed by our preliminary calculation. As demonstrated later, the external field results in formation of Néel, *C*-type and Bloch-like walls, depending on the field strength and direction. In this section, we identify the most stable 180° domain wall structure at zero external field.

As mentioned in the introduction, the type of domain wall essentially depends on the film thickness. The domain wall structure of Fe film with thickness ranging from 30 to 500 nm has been investigated by means of high resolution MFM.[11] It has been revealed that the stable 180° domain wall structure varies from the Bloch-type to the Néel type character with decreasing the film thickness. Several micromagnetic simulations have demonstrated that the *C*-type wall is the most stable in the Fe thin film with a wide range of film thickness, 60–3800 nm.[7,22,24,28] It should be noted that in these experimental and theoretical works, the 180° domain wall separates the domains having the magnetization vector parallel to one of ⟨100⟩ directions. Because of the shape anisotropy, in the present system, the magnetization vector points to the wire direction without the external field and 180° domain wall (normal to [110] direction) separates the domains having the magnetization vectors parallel to $\pm[1\bar{1}0]$ direction.

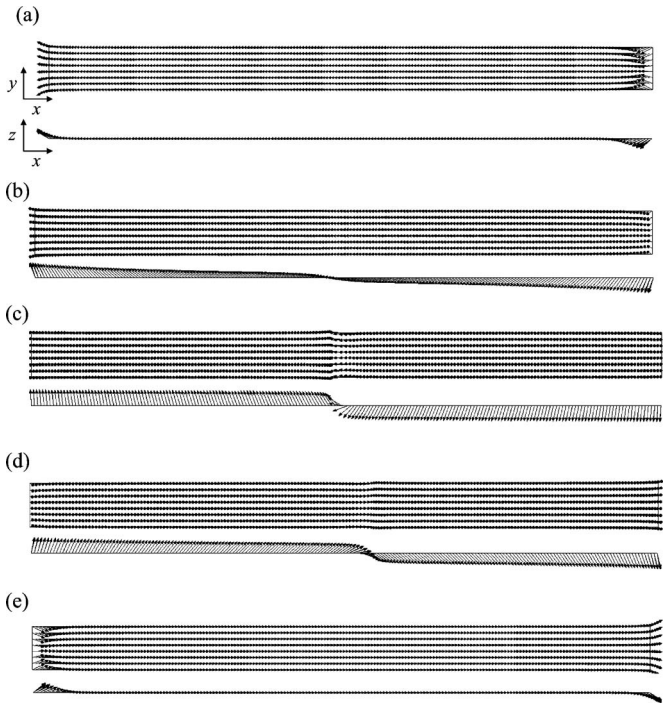

FIG. 3. Magnetization vector distribution during magnetization process ($B_{app,x}$) shown in Fig. 2. (a) −0.5, (b) −0.1, (c) 0.0, (d) 0.05, and (e) 0.5. In each part, the upper panel is the $x-y$ section and the lower panel is the $x-z$ section.

In order to identify the most stable domain wall at zero field, we focus on the system in which a single domain wall exists at the center of the film. One of three possible domain walls, Bloch, Néel, and *C*-type walls was introduced in the system by minimizing the total energy starting from different initial conditions. The calculated total energies of these domain walls are shown in Table I, where the contribution of the exchange, crystalline anisotropy, and the demagnetization energies are also indicated. It is seen that the Néel wall is the most stable domain wall without the external field. As discussed in the following section, the domain wall energy essentially exhibits an anisotropic dependence on the external

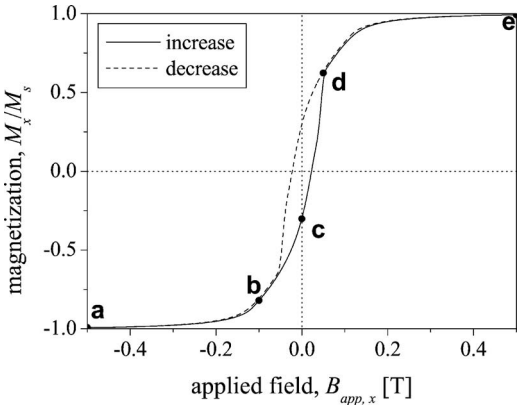

FIG. 2. Hysteresis curve of Fe thin film wire under the external field applied to the x direction. The solid line represents the magnetization process with increasing the external field from −0.5 T and the dashed line indicates the one with decreasing the field from 0.5 T.

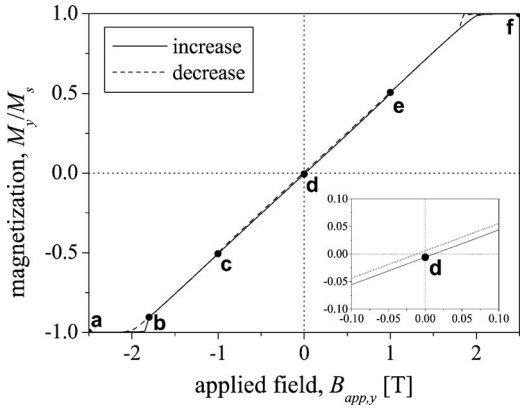

FIG. 4. Hysteresis curve under the external field applied to y direction. The inset is the magnification in the vicinity of the $B_{app,y}=0$. The solid line represents the magnetization process with increasing the external field from −2.5 T, whereas the dashed line indicates the one with decreasing the field from 2.5 T.

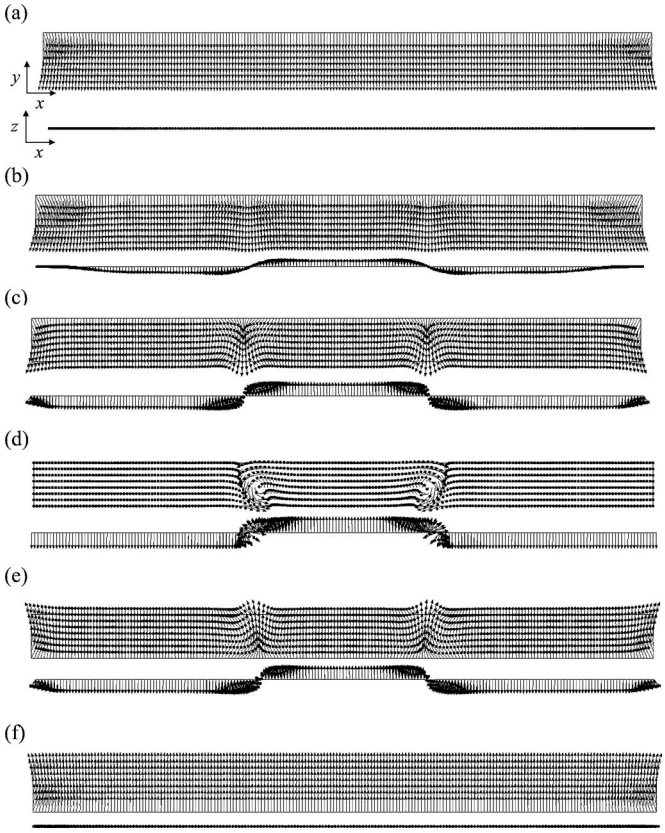

FIG. 5. Magnetization vector distribution during magnetization process ($B_{app,x}$) shown in Fig. 4. (a) −2.50, (b) −1.80, (c) −1.00, (d) 0.00, (e) 1.00, and (f) 2.50. In each part, the upper panel is the $x-y$ section and the lower panel is the $x-z$ section.

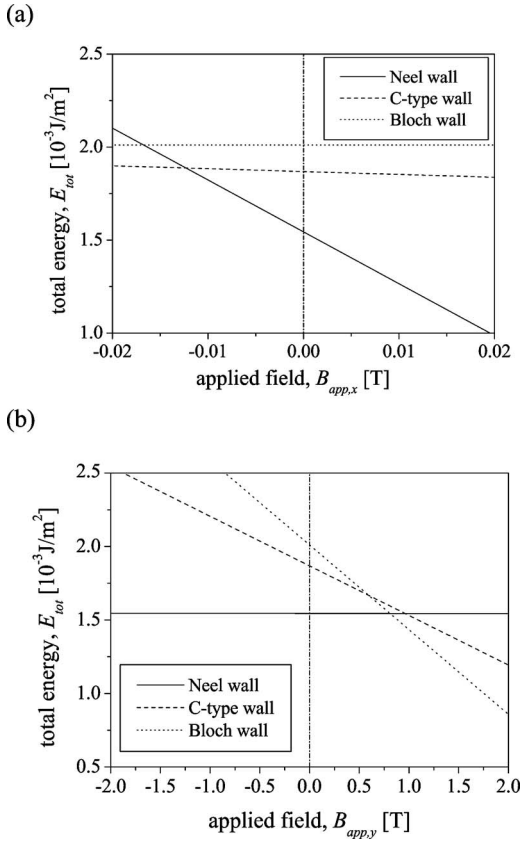

FIG. 7. External field dependence of the domain wall energies per unit area. (a) the external field applied to the x direction and (b) the field applied to the y direction.

field and appearance/disappearance of domain wall and the transition from one to another type of wall are observed during the magnetization reversal process.

B. Magnetization reversal process

Our focus in this section is the magnetization reversal process. First the external field is applied to the width direction of the wire (x direction). The preliminary calculation showed that the external field of 0.5 T is large enough to saturate the wire along the x direction and, therefore, the lower and upper limits of the field were set to be −0.5 and 0.5 T, respectively. The external field is decreased (or increased) with the interval of 0.01 T and the steady state at each field is calculated from the state which corresponds to the steady state at the previous value of field. Starting from various initial micromagnetic states such as random distribution, uniform alignment along the x or z direction, we observed unique hysteresis behavior after one cycle of the external field variation.

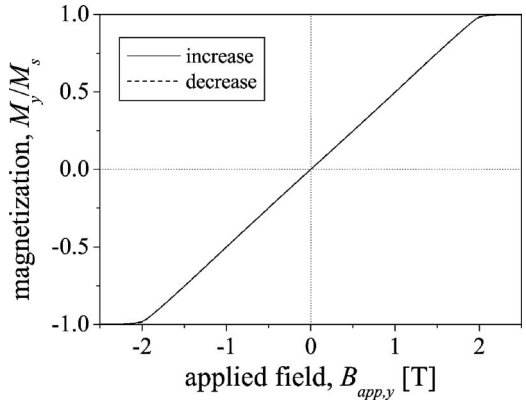

FIG. 6. Hysteresis curve under the external field applied to y direction, but tilted toward the x direction by 2°. The formation of domain wall does not occur and the magnetization vectors over the entire system uniformly rotate during this process.

Figure 2 represent the hysteresis curve of the Fe film wire under the external field in the width direction. Shown in Fig. 3 is the magnetization vector distribution at each external field indicated by black circles in Fig. 2. At $B_{app,x}$= −0.5 T [Fig. 3(a)], the magnetization vectors are uniformly aligned with the $-x$ direction except for the edges where z and y components rise slightly due to the edge effect. One can see that as increasing the external field, the magnetization vectors gradually rotate to the $+z$ and $-z$ directions at the left- and right-hand regions, respectively [Fig. 3(b)], leading to the formation of 180° Néel wall at the center of film [Fig. 3(c)]. Then, the magnetization vectors in both the domains rotate to $+x$ direction [Fig. 3(d)] and 180° Néel wall finally disappears at $B_{app,x}$=0.5 T [Fig. 3(e)]. As one can readily grasp from Figs. 3(a) and 3(e), the formation of Néel wall is a natural consequence of magnetostatic energy relaxation at the wire edges.

Shown in Fig. 4 is the hysteresis curve under the external field in the thickness direction (y direction). Our prelimi-

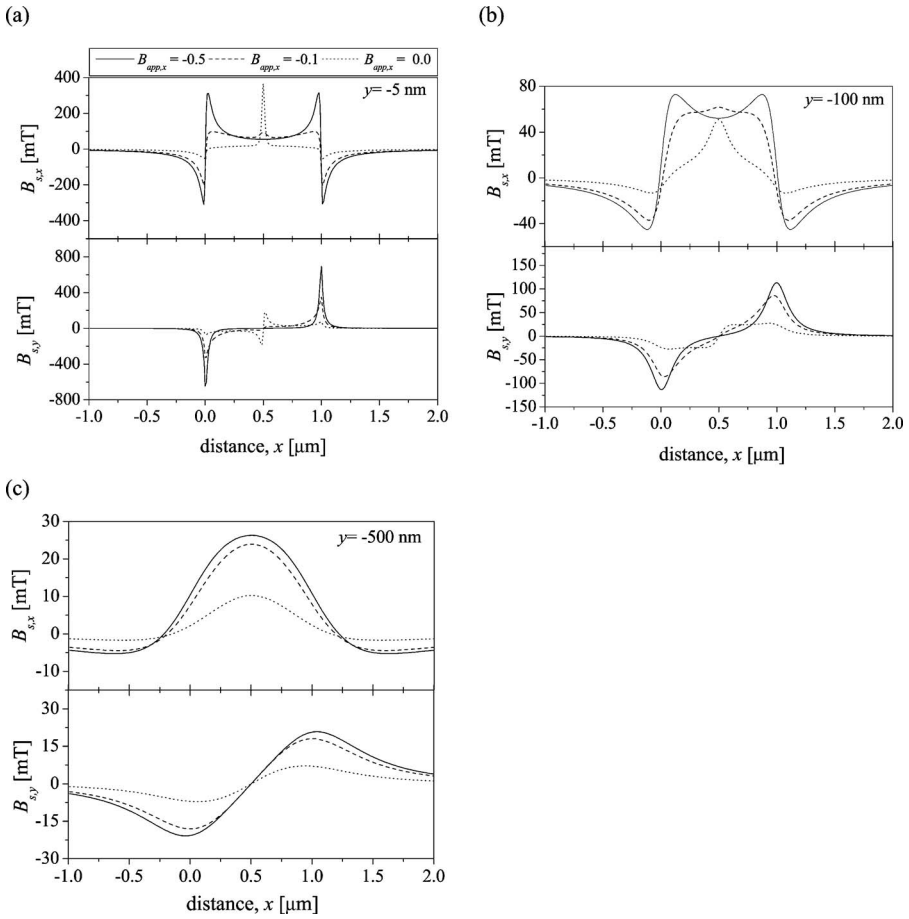

FIG. 8. Spatial profile of stray field at y= (a) −5 nm, (b) −100 nm, and (c) −500 nm originating from the magnetization distributions shown in Fig. 3. In each part, the upper panel indicates the x component of the stray field and the lower panel is y component.

nary calculation showed that in this case, the external field of about 2.0 T is required for the saturation of sample. In this study, the lower and upper limits of the external field were set to be −2.5 and +2.5 T, respectively. The inset in Fig. 4 is a magnification in the vicinity of the $B_{\mathrm{app},y}=0$. One sees quite different hysteresis curve from the one shown in Fig. 2. As increasing the external field from $B_{\mathrm{app},y}=-2.5$ T (solid line), the magnetization first keeps the constant value of −1.0 and then a slight but sharp rising is observed at −1.80 T, followed by nearly linear increment. Figure 5 represents the magnetization vector distributions at the external field indicated by black circles in Fig. 4. At $B_{\mathrm{app},y}=-2.5$ T [Fig. 5(a)], the magnetization vectors are uniformly aligned with the $-y$ direction except for the edges and, then, the magnetic domains having a small magnitude of the z component start to appear with the formation of two Bloch-like walls at $B_{\mathrm{app},y}=-1.80$ T [Fig. 5(b)], which corresponds to the sharp rising portion in the hysteresis curve. One can clearly see that there exist two Bloch-like walls at $B_{\mathrm{app},y}=-1.00$ T. As the external field increases, these domain walls turn into C-type walls to reduce the stray field [Fig. 5(c)]. Further increase of external field gives rise to the transition from the C-type walls to the Bloch-like walls having $+y$ component [Fig. 5(d)] and finally wipes out the domain walls [Fig. 5(e)].

It is to be noted that the hysteresis behavior shown in Figs. 2 and 4 are well known as easy-axis and hard-axis hysteresis behavior, respectively, due to the shape anisotropic effect.[12,15,43,44] Importantly, the external field applied to the width direction yields 180° Néel wall, whereas the field parallel to the thickness direction leads to the formation of 180° C-type and Bloch-like walls. As already mentioned, the formation of the Néel wall, shown in Fig. 3 originates from the magnetostatic energy relaxation at the wire edges. In Fig. 5(a) [Fig. 5(f)], however, the magnetization vectors at edges of both sides are aligned to the $-y$ [$+y$] direction without the z component and, therefore, the formation of Bloch-like domain walls is not ascribable to the magnetostatic energy relaxation at the edges. Although in the preliminary calculation, we observed the same hysteresis behavior shown in Figs. 4 and 5 after one cycle of the external field variation, irrespective of the initial condition for the micromagnetic vector distribution, the formation of two Bloch-like walls is associated with the numerical accuracy. Small fluctuations in orientation of magnetization vector, which is due to the numerical error, trigger the formation of the domain walls in Fig. 5. In fact, the simulations with less numerical accuracy, i.e., with using stopping criterion of $|m_i(t+\Delta t)-m_i(t)| \leq 10^{-3}$ demonstrated that four Bloch-like domain walls appear and turn into C-type walls during the reversal process. In order to avoid the problem with the numerical accuracy, we performed the calculations by tilting the external field to x or z direction by a few degrees. The external field tilted up to 1° to the x or z direction does not yield any change in the calculated results, whereas tilting by 2° leads to the uniform rotation of magnetization vectors over the entire system without the formation of any domain wall. The corresponding magnetization curve is shown in Fig. 6 where there are

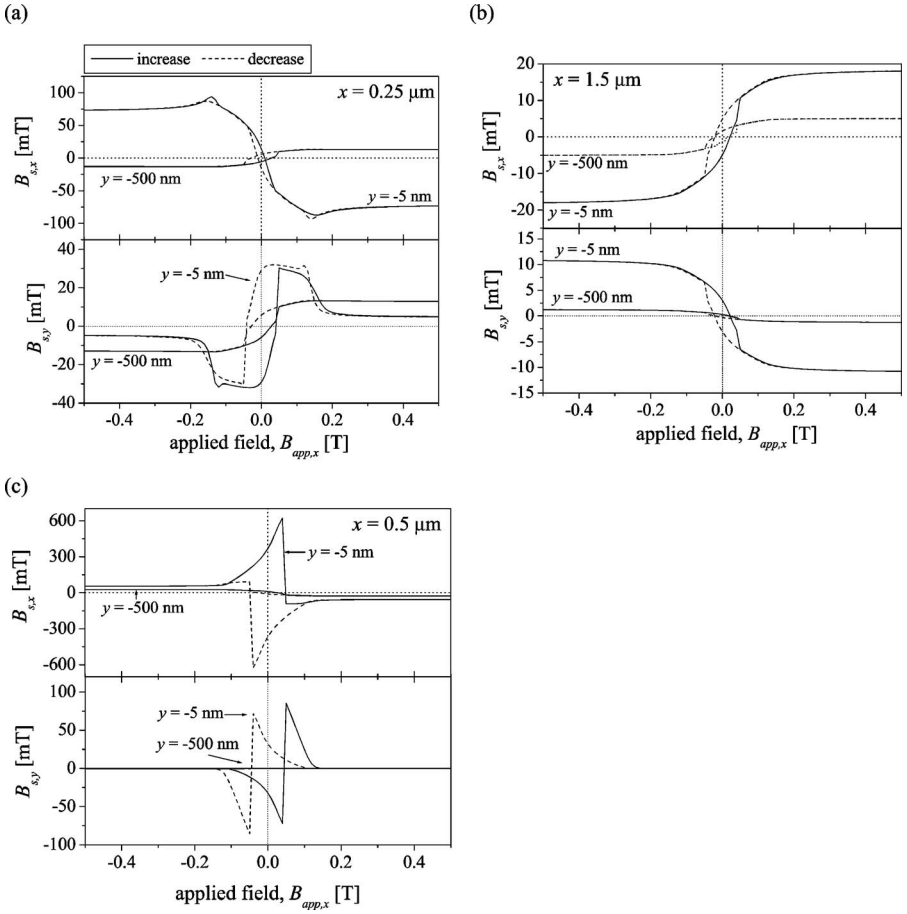

FIG. 9. External field dependence of stray field at x= (a) 0.25 μm, (b) 1.5 μm, and (c) 0.5 μm during the magnetization process shown in Fig. 2. In each part, the upper panel represents x component of the stray field and the lower panel is the y component.

no slight rising portion at $B_{\mathrm{app},y}=1.80$ and virtually no hysteresis behavior, and this magnetization curve should be more appropriate. In reality, however, the thermal fluctuation and structural inhomogeneity may cause the formation of domain walls. The result in Fig. 5 claims that once such domain walls are formed, the character of the wall should be Bloch-like at higher or lower fields and the transition from Bloch-like to C-type walls should take place during the reversal process. Such a field dependency of the stability of domain wall structures is important issue to be further addressed. In this study, hence, our focus is directed to the results shown in Figs. 4 and 5, stating caution that the formation of the domain wall requires some fluctuations and these calculated results involve uncertainty regarding how many domain walls form during the reversal process. In the following, the field dependency of the domain wall structure is discussed based on anisotropic dependence of the wall energy on the direction of the external field.

In Sec. III A, the total energies of 180° Néel, C-type, and Bloch walls at zero external field were demonstrated. Within the present calculation, the total energy of the system consists of the exchange, crystalline anisotropy, demagnetization, and Zeeman energies. In this discussion, for simplicity, we assume that the magnetization vector distribution, i.e., the wall structure is fixed to be the one obtained without the external field in Sec. III A. Then, all the energy contributions except for the Zeeman energy are constants within this simplification. The Zeeman energy contribution, E_{ex}, is explicitly given as

$$E_{\mathrm{ex}} = -\int \mathbf{M}(\mathbf{r}) \cdot \mathbf{B}_{\mathrm{app}} \cdot d\mathbf{r}$$
$$= -V(\langle M_x\rangle_{\mathrm{AV}} B_{\mathrm{app},x} + \langle M_y\rangle_{\mathrm{AV}} B_{\mathrm{app},y} + \langle M_z\rangle_{\mathrm{AV}} B_{\mathrm{app},z}), \quad (1)$$

where V is the volume of the system and $\langle M_i\rangle_{\mathrm{AV}}$ is the spatial average of i component of $\mathbf{M}(\mathbf{r})$ over the whole system. When $\mathbf{M}(\mathbf{r})$ is assumed to be unchanged under the external field, the Zeeman energy and thus the wall energy has the linear dependence on the field and its slope is entirely determined by the averaged magnetization, $\langle M_i\rangle_{\mathrm{AV}}$, over the system with the single wall structure.

Figure 7 shows the field dependence of Néel, C-type, and Bloch wall energies calculated with the above-mentioned simplification. The dependences of energy on $B_{\mathrm{app},x}$ and $B_{\mathrm{app},y}$ are presented in Figs. 7(a) and 7(b), respectively. It should be pointed out that $\langle M_x\rangle_{\mathrm{AV}}$ and $\langle M_y\rangle_{\mathrm{AV}}$ are positive values in all three wall structures employed in this discussion. It is first noticed in Fig. 7 that the wall energies at zero field, $B_{\mathrm{app},x}(B_{\mathrm{app},y})=0$, are identical to those given in Table I. One can readily grasp that the wall energies for these walls have quite different field dependencies. The C-type and Bloch wall energies do not significantly change with the field along the x direction [Fig. 6(a)], whereas the Néel wall structure is substantially stabilized by the field along the $+x$ direction. When $B_{\mathrm{app},x}$ is less than -0.012, the C-type wall energy is lower than the Néel wall energy. It is, however, expected that at $B_{\mathrm{app},x} \leq -0.012$, the Néel wall with negative $\langle M_x\rangle_{\mathrm{AV}}$ should appear, as this wall has much lower energy.

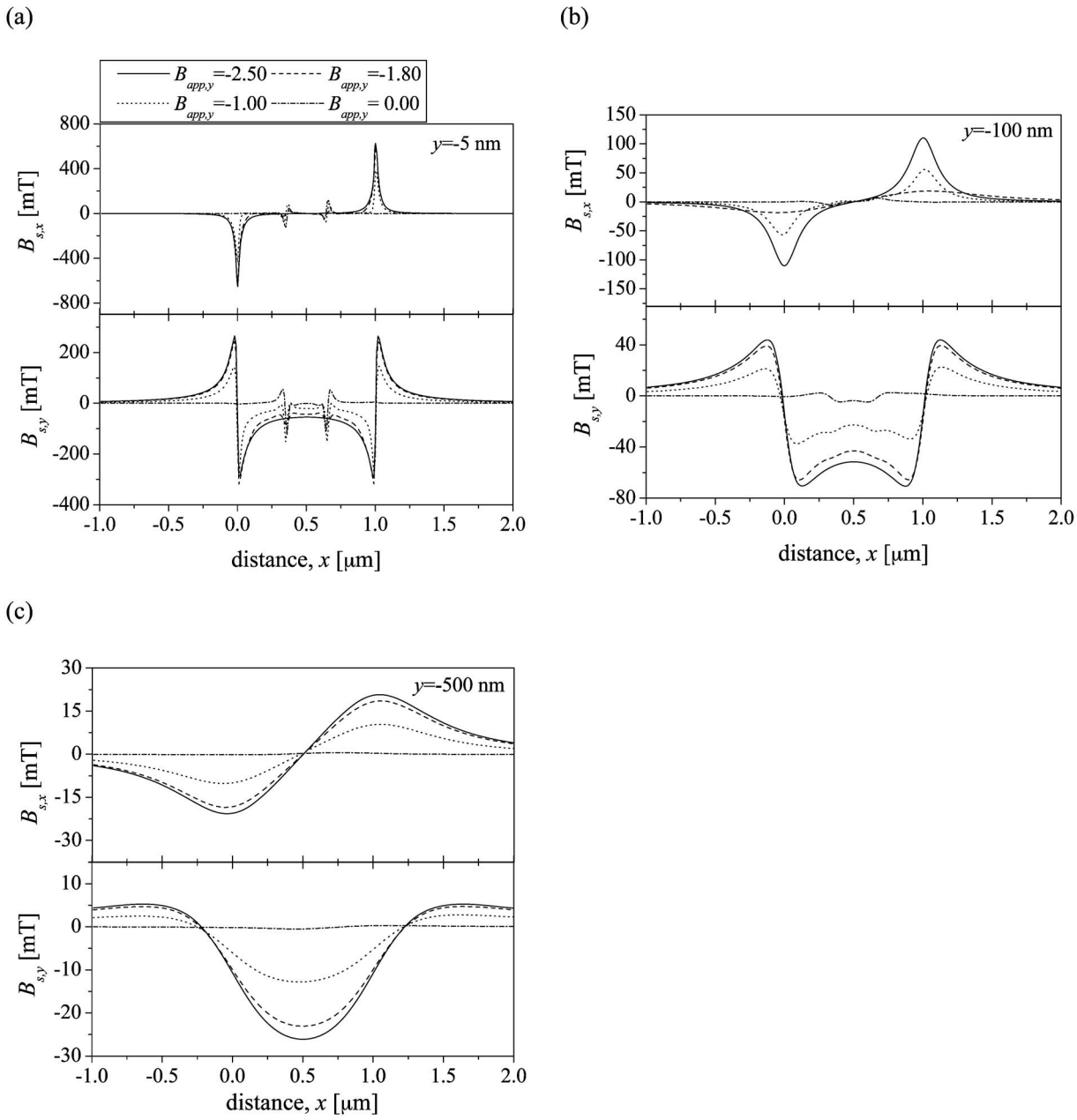

FIG. 10. Spatial profile of stray field at y= (a) −5 nm, (b) −100 nm, and (c) −500 nm originating from the magnetization vector distributions shown in Fig. 5. In each part, the upper panel is the x component of the stray field and the lower panel is the y component.

Such a transition from Néel wall with positive $\langle M_x \rangle_{\mathrm{AV}}$ to the one with negative $\langle M_x \rangle_{\mathrm{AV}}$ is exactly what we observed in Figs. 2 and 3.

When the applied field is parallel to y direction, the Néel wall energy is almost constant and the C-type and Bloch wall energies show strong dependencies [Fig. 7(b)]. At $B_{\mathrm{app},y}=2.0$, both the Bloch and C-type wall energies are much lower than the Néel wall energy and the Bloch wall is the most stable. Although the Néel wall becomes the most stable at $B_{\mathrm{app},y} \leq 0.8$, the domain wall structure does not necessarily relax into the most stable one. The domain wall structure is one of the minimum energy states and, therefore, the transition between the wall structures cannot be discussed based only on the comparison in the wall energy. One point to be mentioned here is that the transition from the Bloch wall to the Néel wall involves a substantial realignment of magnetization vectors, i.e., large rotations of the magnetization vectors over the wall region, compared to the transition from Bloch to C-type walls, which can be understood from the difference in the value of $\langle M_i \rangle_{\mathrm{AV}}$, that is, the slopes of wall energies in Fig. 7. As observed in Fig. 5, the Bloch-like walls change into the C-type walls. A further discussion needs the analysis on possible paths from one type of wall structure to the other type and the comparison between the energy barriers for each path, which are beyond the present concern.

The present discussion is based on the condition that the domain wall structure is invariant under the external field, which, in reality, cannot be satisfied. Within this simplification, however, one can readily grasp the essential point about the external field dependence of wall energy.

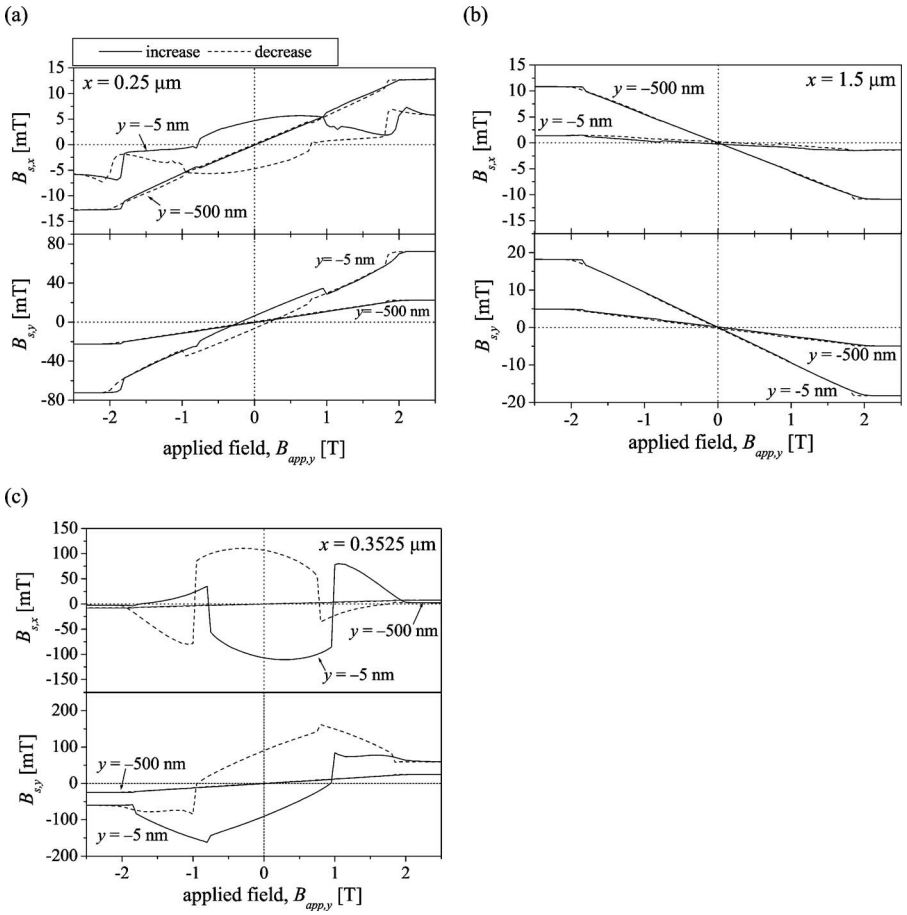

FIG. 11. External field dependence of stray field at x= (a) 0.25 μm, (b) 1.5 μm, and (c) 0.35 μm during the magnetization process shown in Fig. 4. In each part, the upper panel is x component of the stray field and the lower panel is y component.

C. Stray field during magnetization processes

The knowledge about the stray field of ferromagnetic electrodes is indispensable in studying the spin transport phenomena in a spin injection device.[21,45] In addition, such knowledge is a basis in the MFM analysis on the micromagnetic structure.[7,10] In this section, we discuss the stray field behavior resulting from the micromagnetic state shown in the previous sections.

The external field applied to the width direction results in appearance and disappearance of the Néel wall at the center of film as discussed in the Sec. III B. Figure 8 represents spatial profiles of the concomitant stray field at (a) −5 nm, (b) −100 nm, and (c) −500 nm below the Fe thin film wire. In Figs. 8(a)–8(c), the upper and lower parts show the profiles of the x and y components of local stray field, respectively. It is noted that x=0 and x=1 μm correspond to the edges of Fe thin film (see Fig. 1). First, the edge effect is fairly strong at y=−5 nm when the sample is fully magnetized to the $-x$ direction at $B_{\mathrm{app},x}$=−0.5 T. When $B_{\mathrm{app},x}$=0, one can clearly notice the existence of the Néel wall in both the x and y components of the stray field at y=−5 nm [Fig. 8(a)]. This effect drastically becomes week as going far below the wire and, at −500 nm below the wire, this almost completely disappears.

Shown in Fig. 8 is the dependence of the stray field on the external field. In Figs. 8(a)–8(c), the upper and lower parts represents the x and y components of the stray field, respectively. It should be emphasized here that the location of x=0.5 μm corresponds to the center of the Néel wall. It is seen that there exists the hysteresis of stray field at all the spatial points. The range of magnitude of stray fields $B_{s,x}$ and $B_{s,y}$ are quite small, less than 20 mT, at x=1.5 μm [Fig. 9(b)]. The large variation of the stray field at x=0.5 μm and y=−5 nm [Fig. 9(c)] is entirely ascribable to the formation of Néel wall. This effect of Néel wall drastically decreases with going far below the wire and is not substantial at y=−500 nm. The complicated shape of the hysteresis curve at x=0.25 μm and y=−5 nm partly stems from the edge effect.

The external field parallel to the thickness direction may not introduce any domain wall during the reversal process in this wire, as discussed in the Sec. III B. However, the formation of domain walls as shown in Fig. 5, which is associated with the numerical accuracy in the calculation, is likely to occur due to the thermal fluctuation and structural inhomogeneity in reality. In the following, therefore, we focus on the reversal process shown in Figs. 4 and 5 in order to demonstrate the effect of the domain wall formation and transition on the stray field behavior. Figure 10 is the spatial profile of the corresponding stray field below the Fe thin film wire. Again, the edge effect is strong at y=−5 nm when the sample is fully magnetized. The existence of two Bloch-like walls can be seen in stray field at y=−5 nm when the external field is zero and this is invisible at y=−500 nm.

The dependence of stray field on the external field is demonstrated in Fig. 11. It is noticed that the location of x=0.35 μm [Fig. 11(c)] corresponds to the center of the domain wall. The change of the wall structure is quite sensi-

tively observed in the stray field hysteresis at $x=0.35$ μm and $y=-5$ nm [Fig. 11(c)]. For example, as increasing the external field from $B_{\mathrm{app},y}=-2.5$ T, the y component of the stray field $B_{s,y}$ [solid line in lower part of Fig. 11(c)] keeps a constant value and then starts to decrease at $B_{\mathrm{app},y}=-1.80$ T when two Bloch-like walls appear. Then $B_{s,y}$ turns to increase at $B_{\mathrm{app},y}=-0.8$ T where the Bloch-like walls start to turn into the *C*-type wall. The sharp rise of $B_{s,y}$ at $B_{\mathrm{app},y}=1.0$ T corresponds to the transition of the *C*-type walls to the Bloch-like walls. The stray field hysteresis is a sensitive measure of the evolution/devolution of the domain wall structure.

IV. SUMMARY

In the present study, the micromagnetic behavior of the Fe thin film wire, which is one of the effective electrodes for the spin transistor, has been studied on the basis of two-dimensional micromagnetic simulation. First, we identified that the most stable 180° domain wall structure in this film wire at zero field is Néel wall. Our concern was then directed to the external field dependence of the domain wall structure and the corresponding stray field. The external field applied to the width direction results in the formation of Néel wall which is the most stable wall without the field. On the other hand, our calculation showed that the Bloch-like and *C*-type walls are introduced by the external field applied to the thickness direction, although uncertainty is involved in our result regarding the number of domain walls appearing during this process. These behaviors can successfully be comprehended based on the external field dependence of the wall energy. Finally it should be mentioned that in the present simulation, we did not take into account the effects of structural inhomogeneity, thermal fluctuation and an additional uniaxial anisotropy effect due to surface reconstruction of InAs.[46] The explicit consideration of these effects is required for a more realistic and detailed analysis on the micromagnetic state in the Fe film. This remains as a future work.

ACKNOWLEDGMENTS

This work was partly supported by the Next Generation Super Computing Project, Nanoscience Program, and Grant-in-Aid for Scientific Research from MEXT, Japan.

[1] S. Datta and B. Das, Appl. Phys. Lett. **56**, 665 (1990).
[2] G. A. Prinz, in *Ultrathin Magnetic Structures II*, edited by B. Heinrich and J. A. C. Bland (Springer, Berlin, 1994), pp. 1–44.
[3] A. Hirohata, Y. B. Xu, C. M. Gruertler, and J. A. C. Bland, J. Appl. Phys. **85**, 5804 (1999).
[4] C. M. Teodorescu and D. Luca, Surf. Sci. **600**, 4200 (2006).
[5] K. Yoh, H. Ohno, K. Sueoka, and M. E. Ramsteiner, J. Vac. Sci. Technol. B **22**, 1432 (2004).
[6] M. R. Scheinfein, J. Unguris, R. J. Celotta, and D. T. Pierce, Phys. Rev. Lett. **63**, 668 (1989).
[7] M. R. Scheinfein, J. Unguris, J. L. Blue, K. J. Coakley, D. T. Pierce, and R. J. Celotta, Phys. Rev. B **43**, 3395 (1991).
[8] R. Proksch, S. Foss, E. D. Dahlberg, and G. Prinz, J. Appl. Phys. **75**, 5776 (1994).
[9] S. Müller-Pfeiffer, M. Schneider, and W. Zinn, Phys. Rev. B **49**, 15745 (1994).
[10] M. Schneider, St. Müller-Pfeiffer, and W. Zinn, J. Appl. Phys. **79**, 8578 (1996).
[11] E. Zueco, W. Rave, R. Schäfer, M. Mertig, and L. Schultz, J. Magn. Magn. Mater. **196–197**, 115 (1999).
[12] E. Gu, J. A. C. Bland, C. Daboo, M. Gester, and L. M. Brown, Phys. Rev. B **51**, 3596 (1995).
[13] E. Gu, E. Ahmad, S. J. Gray, C. Daboo, J. A. C. Bland, and L. M. Brown, Phys. Rev. Lett. **78**, 1158 (1997).
[14] E. Gu, E. Ahmad, J. A. C. Bland, L. M. Brown, M. Rühring, A. J. McGibbon, and J. N. Chapman, Phys. Rev. B **57**, 7814 (1998).
[15] J. Yu, U. Rüdiger, A. D. Kent, L. Thomas, and S. S. P. Parkin, Phys. Rev. B **60**, 7352 (1999).
[16] S. S. Yan, R. Schreiber, P. Grünberg, and R. Schäfer, J. Magn. Magn. Mater. **210**, 309 (2000).
[17] W. F. Brown, Jr., *Micromagnetics* (Interscience, New York, 1963).
[18] J. Fidler and T. Schrefl, J. Phys. D **33**, R135 (2000).
[19] A. Aharoni, Physica B **306**, 1 (2001).
[20] V. Christoph and R. Schäfer, Phys. Rev. B **70**, 214419 (2004).
[21] M. Barthelmess, A. Thieme, R. Eiselt, and G. Meier, J. Appl. Phys. **93**, 8400 (2003).
[22] A. Aharoni and J. P. Jakubovics, Phys. Rev. B **43**, 1290 (1991).
[23] M. R. Scheinfein, J. Unguris, D. T. Pierce, and R. J. Celotta, J. Appl. Phys. **67**, 5932 (1990).
[24] L. Hua, J. E. L. Bishop, and J. W. Tucker, J. Magn. Magn. Mater. **155**, 49 (1996).
[25] S. Huo, J. E. L. Bishop, and J. W. Tucker, J. Appl. Phys. **81**, 5239 (1997).
[26] S. Huo, J. E. L. Bishop, J. W. Tucker, W. M. Rainforth, and H. A. Davies, J. Magn. Magn. Mater. **177–181**, 227 (1998).
[27] S. Huo, J. E. L. Bishop, J. W. Tucker, W. M. Rainforth, and H. A. Davies, J. Magn. Magn. Mater. **177–181**, 229 (1998).
[28] S. Huo, J. E. L. Bishop, J. W. Tucker, W. M. Rainforth, and H. A. Davies, J. Magn. Magn. Mater. **218**, 103 (2000).
[29] M. Lu and P. J. Leonard, Physica B **365**, 82 (2005).
[30] M. R. Scheinfein and J. L. Blue, J. Appl. Phys. **69**, 7740 (1991).
[31] C. Y. You, J. Appl. Phys. **100**, 043911 (2006).
[32] S. W. Yuan and H. N. Bertram, Phys. Rev. B **44**, 12395 (1991).
[33] L. Thomas, S. S. P. Parkin, J. Yu, U. Rüdiger, and A. D. Kent, Appl. Phys. Lett. **76**, 766 (2000).
[34] M. Redjdal, J. H. Giusti, M. F. Ruane, and F. B. Humphrey, IEEE Trans. Magn. **39**, 2684 (2003).
[35] R. Engel-Herbert, D. M. Schaadt, and T. Hesjedal, J. Appl. Phys. **99**, 113905 (2006).
[36] D. Goll, G. Schütz, and H. Kronmüller, Phys. Rev. B **67**, 094414 (2003).
[37] A. E. LaBonte, J. Appl. Phys. **40**, 2450 (1969).
[38] R. D. McMichael, M. J. Donahue, D. G. Porter, and J. Eicke, J. Appl. Phys. **85**, 5816 (1999).
[39] M. J. Donahue, D. G. Porter, R. D. McMichael, and J. Eicke, J. Appl. Phys. **87**, 5520 (2000).
[40] A. J. Newell, W. Williams, and D. J. Dunlop, J. Geophys. Res. **98**, 9551 (1993).
[41] W. Rave and A. Hubert, IEEE Trans. Magn. **36**, 3886 (2000).
[42] R. Engel-Herbert and T. Hesjedal, J. Appl. Phys. **97**, 074504 (2005).
[43] J. M. Florczak and E. Dan Dahlberg, Phys. Rev. B **44**, 9338 (1991).
[44] E. Ahmad, L. Lopez-Diaz, E. Gu, and J. A. C. Bland, J. Appl. Phys. **88**, 354 (2000).
[45] G. Meier, R. Eiselt, and M. Halverscheid, J. Appl. Phys. **92**, 7296 (2002).
[46] Y. B. Xu, D. J. Freeland, M. Tselepi, and J. A. C. Bland, Phys. Rev. B **62**, 1167 (2000).